IEEE Access
Multidisciplinary | Rapid Review | Open Access Journal

Received 24 October 2023, accepted 7 November 2023, date of publication 9 November 2023, date of current version 20 November 2023.

Digital Object Identifier 10.1109/ACCESS.2023.3331951

RESEARCH ARTICLE

Optimization and Modeling of a Spatial CAM Mechanism for a Two-Dimensional Plunger Electro-Hydraulic Pump

XINGUO QIU[1,2], FUCHENG WANG[1,2], CHANGLONG LI[1,2], BIDA YI[1,2], JIAN RUAN[1,3], AND WEI JIANG[1,2]

[1]College of Mechanical Engineering, Zhejiang University of Technology, Hangzhou 310023, China
[2]Key Laboratory of Special Purpose Equipment and Advanced Processing Technology, Ministry of Education and Zhejiang Province, Zhejiang University of Technology, Hangzhou 310023, China
[3]Key Laboratory of Special Purpose Equipment and Advanced Manufacturing Technology, Ministry of Education & Zhejiang Province, Zhejiang University of Technology, Hangzhou 310014, China

Corresponding author: Xinguo Qiu (xgqiu@zjut.edu.cn)

This work was supported in part by the China Key Research and Development Program under Grant 2022YFE0198900, and in part by the China Natural Science Foundation under Grant 51675482.

ABSTRACT Traditional cam movements in piston pumps follow a non-stopping motion law, resulting in insufficient smoothness in plunger stroke changes. Consequently, this directly impacts the theoretical flow rate of the pump. To address this issue, describes the transition curve of the non-stopping motion law is constructed in this study by using a fivefold B-spline curve. The maximum uncaused velocity and acceleration are considered optimization parameters. Multi-objective optimization of the motion law is conducted using a genetic algorithm, resulting in the generation of a Pareto solution set. Compared to the modified equivalent acceleration (MEA) motion law, the B-spline combined motion law leads to a reduction of 1.39% and 0.86% in the maximum velocity and acceleration characteristic values, respectively. Furthermore, by employing the principle of a single-parameter surface envelope, a mathematical model of the cam surface is developed. The obtained data points are then solved using the double-three times B-spline cam surface interpolation algorithm. Subsequently, the interpolation result is translated into a cam surface model file based on the data structure of the IGES file.The optimization results demonstrate that compared to equal acceleration and deceleration motion laws, the B-spline optimization curve achieves a seamless transition. Specifically, the maximum pressure angle decreases from 27.98° to 19.92°, and the minimum radius of curvature decreases from 9.94 mm to 7.44 mm, validating the accuracy of the theoretical analysis. Experimental displacement tests are conducted on the spatial cam mechanism, revealing that the cam design process has been streamlined, and the designed spatial cam exhibits enhanced fitting performance.

INDEX TERMS Space CAM mechanism, two-dimensional plunger electro-hydraulic pump, B-spline curve, multi-objective genetic algorithm, envelope principle of a single-parameter surface.

I. INTRODUCTION

With the emergence of electrification, the electro-hydrostatic actuator (EHA) [1], [2] in hydraulic transmission technology has gained significant attention as a research focus. As early as the 1980s, Europe and the United States conducted extensive prototype testing and flight verification of the EHA actuation system, demonstrating a series of advantages associated with the EHA actuation approach. Currently, EHA actuation technology has been successfully deployed in controlling the main control rudder surface of prominent aircraft, such as the U.S. F-35 fighter jet and Airbus A380 airliner [3]. Compared to traditional hydraulic actuation technology, EHA actuation technology offers numerous advantages, primarily in terms of streamlined system structure, optimized resource allocation, enhanced energy efficiency, improved

The associate editor coordinating the review of this manuscript and approving it for publication was Christian Pilato.

power-to-weight ratio, heightened reliability, testability, maintenance, and reduced overall lifetime cost. Moreover, the inherent electric actuation capability of EHA technology aligns well with the development requirements of future multi-electric/all-electric warplanes, making it the preferred direction for the airborne actuation system of advanced aircraft in the future.

Electro-hydraulic pumps play a crucial role in EHA technology. To effectively meet the demands of future EHA operations, electro-hydraulic pumps must satisfy elevated criteria, including increased speeds, higher pressures, and enhanced integration capabilities. Furthermore, they should be made to minimize transmission losses and offer extended reliability and lifespan [4]. To ensure optimal system performance and stability under a diverse range of operating conditions, it is imperative to develop electro-hydraulic pumps that are capable of effectively addressing various scenarios. By doing so, we can ensure that the electro-hydraulic pumps are equipped to handle different operating conditions while maintaining consistent and reliable system operation.

Currently, the research and development of hydraulic electro-hydraulic pumps has emerged as a prominent area of study [5], [6]. The research focuses on optimizing the structure of the electro-hydraulic pump, including optimizing the motor [7] and innovating the pump design [8], [9]. Additionally, efforts are being made to enhance the operating environment of the electro-hydraulic pump [10] and improve its stability during usage [11]. The two-dimensional plunger electro-hydraulic pump comprises a motor, a coupler, and a two-dimensional piston pump. The pivotal component of the two-dimensional piston pump is the spatial cam, which directly determines the plunger's movement stroke and significantly impacts the pump's performance in terms of vibration, noise, lifespan, and reliability.

By examining the operational principle of the two-dimensional (2D) piston pump [12], [13], [14], it becomes apparent that the piston undergoes axial reciprocating displacement twice during a rotational cycle without coming to a halt at either end. Consequently, the motion of the cam follower should adhere to a non-stop motion law, with equal angles for both the pushing and returning motions. Various algebraic formulas have been commonly employed to express the cam mechanism for the non-stop motion law. Detailed descriptions of these formulas can be found in the literature on cam mechanisms [15]. Examples of such formulas include equal acceleration and equal deceleration, modified trapezoidal, modified sinusoidal, modified isotropic, and other motion laws. With the advancement of curved surface technology, some experts and scholars have proposed utilizing spline curves to design follower motion laws. Scholars such as Angeles [16], Tsay [17], Qiu [18], and others have utilized spline curves to design and optimize cam motion laws.

In the realm of cam surface construction, Tsay et al. [19]. applied the single-parameter surface family envelope theory to formulate a mathematical model for spatial cam surfaces. They proposed a solution approach capable of addressing diverse planar and spatial cam scenarios. Jin Dingcan [20] developed a spatial cam mathematical model grounded in contact relationships, enabling the calculation of surface data points through spatial contact considerations.

In this study, the B-spline curve serves as the transitional segment for the combined non-stop motion law. This choice is made to effectively address instances where spatial cam mechanisms exhibit continuous impact while using solely equal acceleration and equal deceleration motion laws. By employing a multi-objective genetic algorithm, the B-spline curve can be optimized to yield a motion law boasting comprehensive performance. The optimized B-spline curve exhibits a smooth and natural fitting characteristic, which leads to reduced losses and noise in bearings and transmission systems. Additionally, it significantly enhances transmission efficiency and prolongs the lifespan of the mechanism.Through the MATLAB GUI toolbox, a spatial cam design program is developed. The program establishes a mathematical model for cam surfaces via the single-parameter surface envelope principle. By adhering to the IGES file's data structure, the cam surface model is acquired and subsequently verified through simulations and experiments. This approach visualizes cam mechanism designs, mitigating design challenges and reducing cycle times.

II. COMPOSITION AND WORKING PRINCIPLE

The 2D plunger electro-hydraulic pump represents a tightly interconnected system encompassing a permanent magnet synchronous motor, a coupler, and a 2D plunger pump. To offer a clearer understanding of the electro-hydraulic pump's structural configuration, a cross-sectional view of the two-dimensional plunger electro-hydraulic pump is presented in FIG 1. The mechanical arrangement can be outlined as follows:

The coupler is securely linked to the rotor, leading to enhanced efficiency in transferring mechanical energy. This connection propels the regular movement of the plunger shaft.

Within the hollow rotor shaft, the two-dimensional electro-hydraulic pump is installed, resulting in a significant reduction in the axial dimensions required for the device. This setup substantially heightens the integration level of the electro-hydraulic pump.

For structural support, the left side of the pump body is sustained through the interaction between the outer spline on the plunger shaft and the inner spline of the coupler. On the right side of the pump body, support is achieved through the connection between the shoulder of the pump casing and the front cover. By employing these two distinct support methods in tandem, the pump body is effectively secured in place, ensuring reliable fixation.

Fig 1 shows a visual representation of this arrangement.

The operational principle of the 2D electro-hydraulic pump is described as follows: upon energizing the pump, a three-phase current is introduced into the symmetrical windings

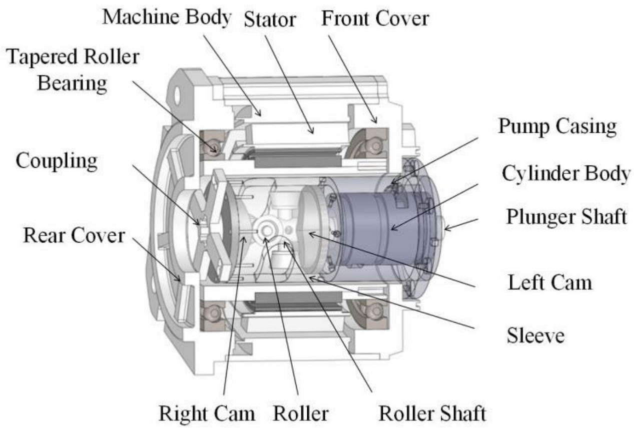

FIGURE 1. Structure diagram of a two-dimensional plunger-type hydraulic pump.

of the stator. This infusion generates a consistent amplitude stator rotating magnetic field. This magnetic field is then conveyed to the coupler, which is firmly interconnected with the stator. The coupler subsequently impels the rotation of the rotor, thereby transmitting torque to the plunger shaft of the two-dimensional piston pump. This torque prompts the initiation of rotational motion in the plunger shaft.

By adhering to the constraints of the space cam mechanism, the plunger shaft exhibits circumferential rotation while concurrently undergoing axial reciprocating linear motion. This combined movement dynamic is pivotal in driving the normal functioning of the 2D piston pump.

Functioning as a pivotal mechanism to actualize the dual degree of freedom exhibited by the pump shaft, the performance of the space cam mechanism stands as a determining factor influencing the comprehensive performance, efficiency, and operational lifespan of the motor pump. This mechanism's performance carries significant theoretical research significance and offers substantial potential for diverse engineering applications.

III. MULTI-OBJECTIVE OPTIMIZATION OF THE KINEMATIC CHARACTERISTICS OF THE TWO-DIMENSIONAL SPATIAL CAM MECHANISM IN PISTON PUMPS USING B-SPLINES

A. REPRESENTATION OF THE COMBINATORIAL NON-STOP MOTION LAWS

Combinations of the non-stop motion laws typically stem from the integration of individual motion laws. These often encompass three segments, each of equal time length: equal acceleration, transition curve, and equal deceleration. This configuration ensures the consideration of both the maximum velocity and maximum deceleration. For example, in the context of the modified trapezoidal motion law, a sinusoidal motion law is interpolated between the equal acceleration and equal deceleration segments. This strategic addition prevents abrupt acceleration shifts within the motion law.

In applications necessitating cam motion laws for high-speed scenarios, it is imperative that displacements, velocities, and accelerations at transition points remain devoid of abrupt shifts. This imperative ensures motion continuity, averting both rigid and flexible impacts.

Given its adaptable versatility, the B-spline frequently serves as the transition curve within combined non-stop motion laws. Within this methodology, B-splines act as transition curves, conjoined with other motion laws. The acceleration profile of the combined non-stop motion law, incorporating B-splines, is depicted in Fig 2.

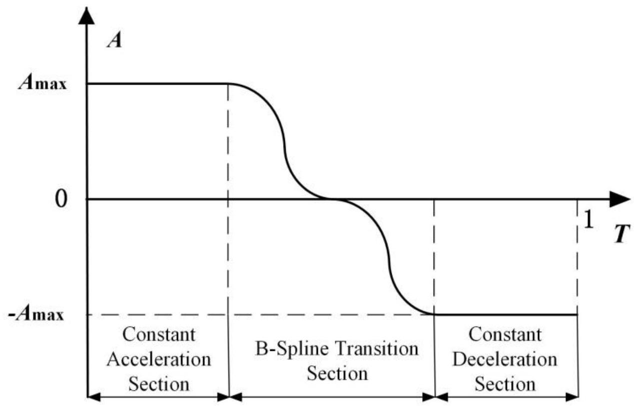

FIGURE 2. Acceleration curve of the B-spline composite uninterrupted motion law.

The incorporation of B-splines into the non-stop motion law, alongside its factorless displacement equation, is represented by the following expression:

$$S = \begin{cases} C_1 T^2, T \in [0, T_1] \\ BS(T), T \in [T_1, T_2] \\ -C_2(T-1)^2 + 1, T \in [T_2, 1] \end{cases} \tag{1}$$

In the equation, C is the quadratic term within the isoacceleration section; BS is the B-spline transition segment function; and T1 is the factorless time of the isoacceleration segment.

Deriving terms from (1) leads to equations describing the factorless velocity, acceleration, and leptokurticity. The characteristic values of S1, situated at the termination of the equal acceleration section, are outlined as follows:

$$\begin{cases} s_1 = CT_1^2 \quad & s_2 = 1 - CT_1^2 \\ v_1 = 2CT_1 \quad & v_2 = 2CT_1 \\ a_1 = 2C \quad & a_2 = -2C \end{cases} \tag{2}$$

To maintain the follower's motion continuity and prevent abrupt rigid or flexible shocks, it is imperative to ensure that the displacement, velocity, and acceleration at both the initial and final points of the transition segment curve do not undergo sudden changes. As elucidated by (2), this requirement not only governs the coordinates of the start and end points of the transition segment but also enforces constraints on the velocity and acceleration at these points. The quintic B-spline interpolation curve is a pertinent choice due to its inherent attributes allowing specification of the initial and end positions as well as the first- and second-order derivatives. Hence, it is adeptly adopted as the transition segment curve for the non-stop motion law.

B. MODELING OF THE QUINTIC B-SPLINE

The piecewise representation of the kth degree B-spline curve equation [21] is represented as follows:

$$\boldsymbol{p}(u) = \sum_{i=0}^{n} \boldsymbol{d}_i N_{i,k}(u) = \sum_{j=i-k}^{k} \boldsymbol{d}_k N_{i,k}(u),\ u \in [u_i, u_{i+1}] \subset [u_k, u_{n+1}] \tag{3}$$

In this equation, di (i=0,1,...,n) represents the control vertices, and Ni,k(u) denotes the k-th degree canonical B-spline basis function determined by the node vector U according to the de Boor-Cox recurrence formula. The recurrence relation equation for Ni,k(u) is as follows:

$$\begin{cases} N_{i,0}(u) = \begin{cases} 1 & u_i < u < u_{i+1} \\ 0 & \text{else} \end{cases} \\ N_{i,k}(u) = \frac{u-u_i}{u_{i+k}-u_i} N_{i,k-1}(u) \\ + \frac{u_{i+t+1}-u}{u_{i+t+1}-u_{i+1}} N_{i+1,k-1}(u) \\ \text{determine} \frac{0}{0} = 0 \end{cases} \tag{4}$$

The node vector U=[$u_0, u_1, \ldots, u_{n+k+1}$] is defined. To obtain the normalized internal node values, we set $u_0 = u_1 = \ldots = u_k = 0$ and $u_{n+1} = u_{n+2} = \ldots = u_{n+k+1} = 1$, following the concept of a normalized node vector. The computation for obtaining these internal node values is as follows:

$$u_{i+k} = u_{i+k-1} + \Delta p_i \quad , i = 1, 2, \cdots, n-1 \tag{5}$$

Here, Δp_i represents the forward difference vector, which can be expressed using the following formula: $\Delta p_i = \frac{p_i - p_{i-1}}{s}$, where s represents the sum of the distances between adjacent data points.

The solution of the B-spline curve can be classified into the following two categories: the first category is the direct problem, which involves determining the points on the curve based on known control vertices; the second category is the inverse problem, which involves determining the control vertices of the curve based on known data points on the curve. In this paper, the solution of the transitional segment curve belongs to the second category of inverse problems, where we aim to determine n=m+k-1 control vertices (d_i) that pass through $m+1$ given data points P_i (i=0,1,...,m).

By leveraging the local property of the B-spline and the de Boor-Cox recurrence formula, the matrix expression for the 5th degree B-spline function of Segment i can be derived as follows:

$$p_i(u) = \sum_{i}^{i+5} d_i N_{i,k}(u),\ u \in [u_i, u_{i+1}] \subset [u_5, u_{n+1}] \tag{6}$$

According to the requirement of curve interpolation, the endpoint of Segment i is defined as the starting point of Segment i+1 and should be equal to the data point it passes through, which can be represented as $P_{i+1} = p_i(1) = p_{i+1}(0)$. By substituting the m+1 data points Pi into the equation, the linear equation system can be rewritten in matrix form, yielding (7), as shown at the bottom of the next page.

The matrix in (7) contains a total of m+1=n-3 equations. However, a B-spline curve has n+1 control vertices, which means that the number of unknowns exceeds the number of equations. To ensure a unique solution, it is necessary to add four constraint equations. These constraints ensure that the curve's velocity and acceleration at the start and end points of the transition segment are the same as the characteristic values of the beginning of the equal acceleration segment and the end of the equal deceleration segment. Therefore, the four constraints for the velocity and acceleration of the B-spline transition segment's start and end points can be expressed as follows:

$$\begin{aligned} p'(0) = v_s = 2CT_1 \quad p'(1) = v_e = 2CT_1 \\ p''(0) = a_s = 2C \quad p''(1) = a_e = -2C \end{aligned} \tag{8}$$

In this equation, v_s and v_e represent the velocities at the start and end points, respectively; and a_s and a_e represent the accelerations at the start and end points, respectively.

Since the B-spline curve with a duplicate degree of k at both ends has its start and end control points coinciding with the start and end data points, we can derive the first and second derivatives at the start and end data points using the recurrence formula for the r-th derivative of the vector pr(u) at a point on the B-spline curve. The expressions for the first and second derivatives at the start and end data points are as follows:

$$\begin{cases} \dot{p}_0 = \dot{p}_0(u_k) = \sum_{j=k-k+1}^{n} d_j^1 N_{j,k-1}(u_k) = d_1^1 = k\dfrac{d_1 - d_0}{u_{k+1} - u_1} \\ \ddot{p}_0 = \dot{p}_0(u_k) = \sum_{j=k-k+2}^{n} d_j^2 N_{j,k-2}(u_k) = d_2^2 \\ \dot{p}_n = \dot{p}_n(u_{n+k}) = \sum_{j=n+k-1-k+1}^{n+k-1} d_j^1 N_{j,k-1}(u_{n+k}) = d_{n+k-1}^1 \\ \ddot{p}_n = \ddot{p}_n(u_{n+k}) = \sum_{j=n+k-1-k+2}^{n+k-1} d_j^2 N_{j,k-2}(u_{n+k}) = d_{n+k-1}^2 \end{cases} \tag{9}$$

By combining the four aforementioned constraint equations with the matrix, we can solve and obtain all the control points d_i (i = 0,1,..., n) of the B-spline curve. With the B-spline equation and the derivative calculation formula, we can calculate the expressions for the displacement, velocity, acceleration, and jump of the transition curve.

C. FILE FORMATS FOR GRAPHICS

To ensure that the combined motion laws based on B-splines have good kinematic characteristics, a multi-objective genetic algorithm is implemented in this method to optimize the selection of data points for B-spline interpolation. Through this approach, the optimal selection of data points can be obtained to obtain superior motion laws and meet the requirements of the cam design.

1) MULTI-OBJECTIVE OPTIMIZATION PROBLEM OF MOTION LAWS

Given a multi-objective optimization problem, the objectives are often mutually constrained, and it is generally not possible to find a single optimal solution that simultaneously optimizes all objectives. Instead, a set of solutions, known as the Pareto optimal solution set, is obtained. The Pareto optimal solution set includes solutions that do not worsen any objective without compromising at least one other objective. The mathematical model for a multi-objective optimization problem is represented as follows:

$$\begin{aligned} &\min S(x) = \min\left[S_1(x), S_2(x), \cdots, S_f(x)\right] \\ &g_j(x) \leqslant 0, \quad j = 1, 2, \cdots, p \\ &h_k(x) = 0, \quad k = 1, 2, \cdots, l \end{aligned} \tag{10}$$

In this equation, $S_i(x)(i = 1,2,\ldots, f)$ represents the objective functions, $g_j(x)(j = 1,2,\ldots, p)$ represents the inequality constraints, and $h_k(x)(k = 1,2,\ldots, l)$ represents the equality constraints.

The multi-objective optimization for cam motion laws refers to improving the kinematic and dynamic characteristics of cam motion laws without altering the geometric and constraint conditions. These motion laws are applied to a two-dimensional plunger pump, where the influence on the performance of the individual plunger pump needs to be considered in addition to the cam mechanism itself. The flow pulsation and the inertia force experienced by the mechanism in an individual two-dimensional plunger pump are directly proportional to the maximum dimensionless velocity ($V_{\max}$) and maximum dimensionless acceleration ($A_{\max}$) of the motion law. To balance the pump's performance and cam mechanism's kinematic characteristics, the optimization objectives are defined as follows:

$$\begin{cases} S_1(x) = V_{\max} \\ S_2(x) = A_{\max} \end{cases} \tag{11}$$

The maximum velocity and acceleration of the non-stop composite curve that is investigated in this study occur at the midpoint of the pushing stroke segment and the beginning of the transition curve, respectively. The acceleration in the B-spline transition segment should be smaller than the acceleration at the starting point. Moreover, the characteristic values of the existing motion law are used as constraints for the maximum velocity and jump. Therefore, the inequality constraints $g_i(x)$ are defined as follows:

$$\begin{cases} g_1(x) = V_{\max} - 1.84 \leq 0 \\ g_2(x) = A_{\max} - 2C \leq 0 \\ g_3(x) = J_{\max} - 80 \leq 0 \end{cases} \tag{12}$$

In this equation, C represents the quadratic coefficient of the equal acceleration segment.

The displacement, velocity, and acceleration of the endpoints of the transition curve are ensured by B-spline interpolation, so no additional equality constraints are introduced.

2) SOLUTION PROCESS OF THE NSGA-II GENETIC ALGORITHM

The NSGA-II algorithm, proposed by Srinivas and Deb based on the NSGA algorithm, incorporates an elitist strategy that preserves the superior individuals from the parent population. It employs a fast non-dominated sorting technique that reduces the time complexity and introduces a crowding distance and crowding comparison operator as criteria for comparing individuals within the same non-dominated front. This ensures population diversity and makes it a commonly used optimization algorithm for multi-objective optimization problems [22], [23].

The NSGA-II algorithm is used to optimize the motion curve of the cam follower component with the maximum dimensionless velocity and acceleration as optimization objectives. The solution process of the CAM multi-objective genetic algorithm using NSGA-II is illustrated in FIG 3.

The solution process of the CAM multi-objective genetic algorithm is described as follows:

For symmetric non-stop motion laws, the motion curve of the pushing stroke segment is symmetric about the midpoint of the stroke. Given the data points of the first half of the stroke, the data points of the second half can be obtained by utilizing the central symmetry. To reduce the number of optimization variables and speed up the iteration process, the population encoding is defined by using the central symmetry relationship as follows:

$$[C, x_0, x_1, y_1, \ldots, x_m, y_m] \tag{13}$$

$$\begin{bmatrix} p_0 \\ p_1 \\ p_2 \\ p_3 \\ \vdots \\ p_m \end{bmatrix} = \begin{bmatrix} 1 & & & & & \\ & N_{1,5}(u_6) & \cdots & N_{5,5}(u_6) & & \\ & & N_{2,5}(u_6) & \cdots & N_{5,5}(u_6) & \\ & & \ddots & \ddots & \ddots & \\ & & N_{m-1,5}(u_{n+4}) & \cdots & N_{m+3,5}(u_{m+4}) & \\ & & & & & 1 \end{bmatrix} \begin{bmatrix} d_0 \\ d_1 \\ d_2 \\ d_3 \\ \vdots \\ d_m \end{bmatrix} \tag{7}$$

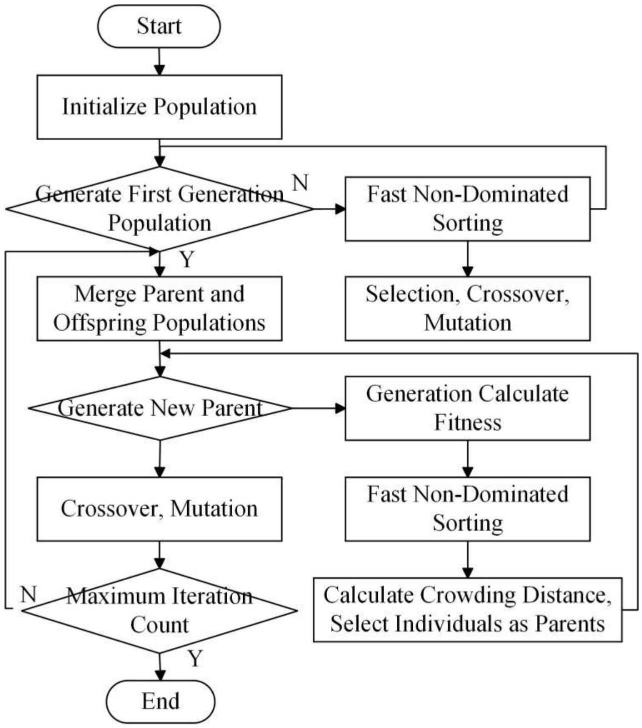

FIGURE 3. **Flowchart of the multi-objective genetic algorithm solution process.**

In this equation, C represents the quadratic coefficient of the equal acceleration segment; x_0 represents the abscissa at the beginning of the B-spline transition segment; and x_i and y_i ($i = 1,2,\ldots, m$) represent the data points of the first half segment.

The solution process of the CAM multi-objective genetic algorithm is as follows:

(1) Initially, a parent population P_0 is randomly created. The non-dominated fast sorting algorithm is used to sort P_0, and tournament selection and genetic operators are used to generate a subpopulation C_0 of size N.

(2) The parent population P_i is merged with the subpopulation C_i to create a merged population R_i with a size of 2 N. The fast non-dominated sorting algorithm is applied to sort the population R_i, assigning each individual a non-dominated rank. For individuals in the same non-dominated front, the crowding distance is used to prioritize their ordering, ensuring diversity among non-dominated individuals within the same rank. After determining the non-dominated rank and crowding distance for each individual, the individuals in R_i are selected based on a sorting criterion that favors individuals with a lower non-dominated rank and a larger crowding distance. The top N individuals are chosen as the new parent population P_{i+1}.

(3) A new subpopulation C_{i+1} is generated using the genetic operators.

(4) Steps 2 and 3 are repeated until the maximum number of iterations is reached, resulting in the Pareto solution set that satisfies the constraint conditions.

D. FILE FORMATS FOR GRAPHICS

Using $V_{\max}$ and $A_{\max}$ as objective functions and (12) as the constraint condition, the number of data points in the first half of the stroke is set to 5, and the data points in the second half are calculated using the central symmetry relationship. The number of optimization variables is 10, and the maximum number of iterations is set to 200 generations. The selection method is tournament selection, with a crossover probability of 0.8 and a mutation probability that is obtained by using Gaussian mutation. The NSGA-II algorithm is employed to perform multi-objective optimization on the data points passed through a fifth-order B-spline interpolation curve. The resulting Pareto front is shown in FIG 4.

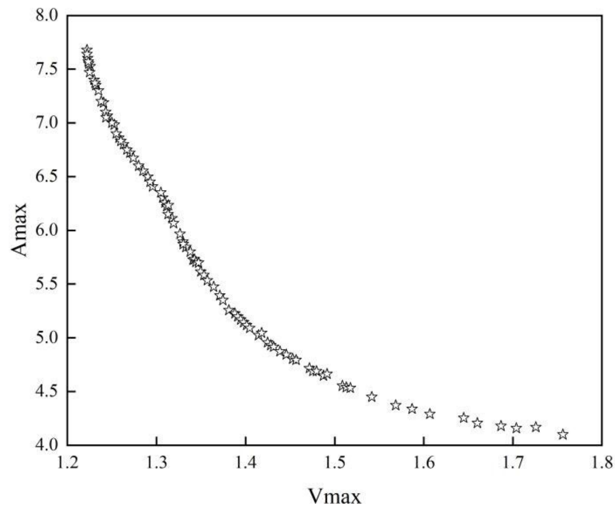

FIGURE 4. **Pareto front of B-spline transition curve optimization.**

As shown in FIG 4, among the Pareto optimal solution set, the leftmost individual has the smallest $V_{\max}$ and the largest $A_{\max}$. At this point, the CAM mechanism has the least momentum, and the flow pulsation of the two-dimensional plunger pump is minimized. However, it experiences the greatest inertia force. Conversely, the rightmost individual has the largest momentum and flow pulsation, but the inertia force is minimized. From the optimization results, it is evident that $V_{\max}$ and $A_{\max}$ have an inverse relationship.

To further analyze the results, the individual with the smallest $V_{\max}$ value from the Pareto optimal solutions is selected, and the dimensionless velocity, acceleration, lift, and dynamic torque curves are obtained, as shown in FIG 5.

Based on FIG 6, a fifth-order B-spline interpolation curve can be used to obtain the displacement, velocity, and acceleration curves that satisfy the specified endpoints. There are no rigid or flexible impacts at the transition point, demonstrating the rationality of using a fifth-order B-spline interpolation curve as the transition segment in non-stop motion laws.

A comparison table (Table 1) is provided below, showing the maximum velocity and acceleration values of the aforementioned individual compared to the characteristics of the modified equivalent acceleration (MEA) motion law:

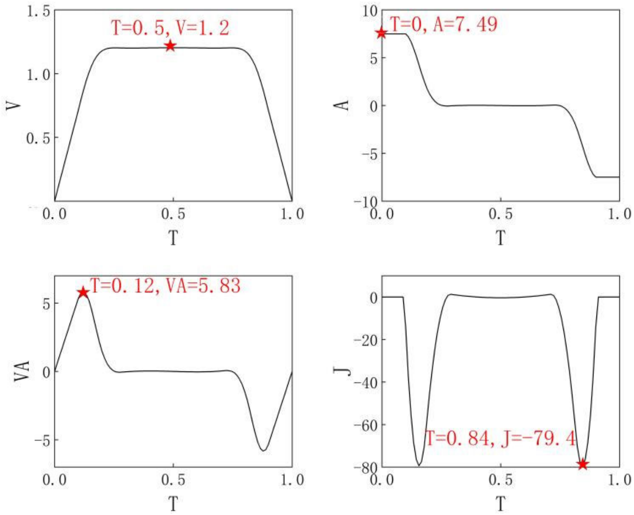

FIGURE 5. Velocity, acceleration, jerk, and dynamic torque curves of the optimal individual Vm.

TABLE 1. Comparison table of the characteristic values of the optimal Vm and MEA.

Motion Law of the Follower	$V_{\max}$	$A_{\max}$
MEA	1.222	7.678
B-Spline Composite Motion Law	1.205	7.612

Table 1: Comparison of the Characteristic Values between Optimal Individuals of the B-Spline Composite Motion Law Vm and MEA.

Based on the data presented in the table, we can conclude that the B-spline composite motion law performs better than the MEA motion law in terms of the maximum velocity and acceleration characteristics. The maximum velocity and acceleration values were reduced by 1.39% and 0.86%, respectively. This indicates that the NSGA-II algorithm can conduct multi-objective optimization on the data points passed through the B-spline transition curve, resulting in motion laws that are superior to analytical expressions.

IV. DESIGN OF SPATIAL CAMS

A. PRINCIPLE OF SINGLE-PARAMETER SURFACE ENVELOPING

The cam surface is a surface envelope formed by the surface family of the follower at different positions as the cam rotates around its own axis for one revolution. In a Cartesian coordinate system, the parameterized single-parameter surface family $\{S_\xi\}$ can be expressed as:

$$r = r\left(u_1, u_2, \varsigma\right) \tag{14}$$

In the equation, u_1 and u_2 represent the surface parameters on the surface family, and ξ represents the parameter variable of the surface family, corresponding to different surfaces Sξ in the surface family.

For each surface S_ξ in the surface family $\{S_\xi\}$, there exists a point P_ξ on Surface S such that S_ξ and S share the same tangent plane at the common point P_ξ. Surface S is then referred to as the envelope of the single-parameter surface family $\{S_\xi\}$. The envelope surface satisfies the following equation:

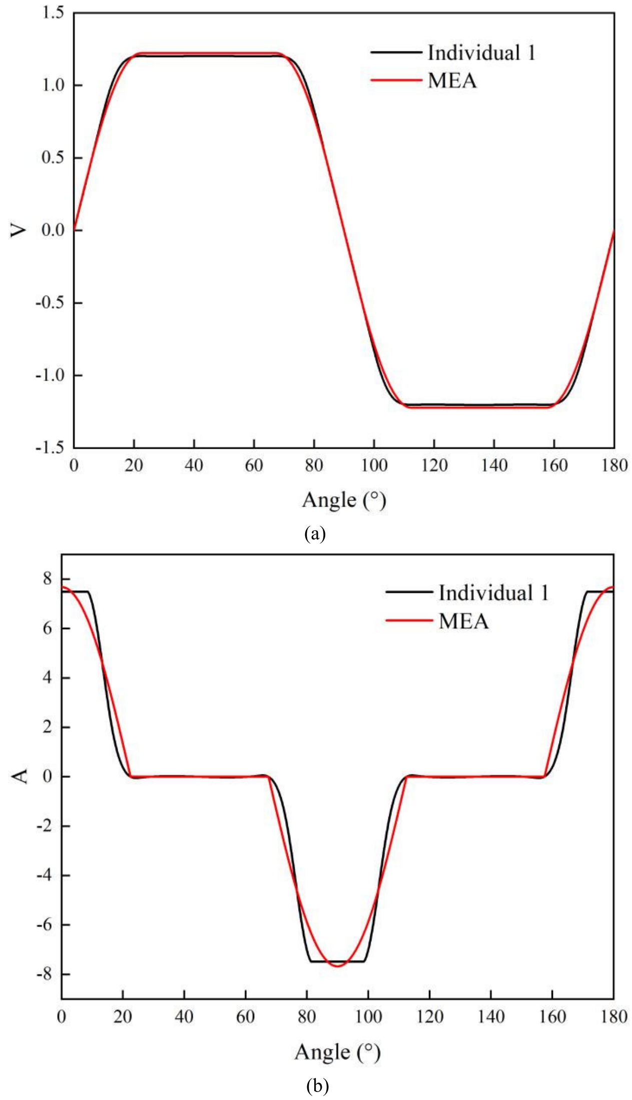

FIGURE 6. Comparison of the dimensionless parameters between individual 1 and MEA (a) Comparison of the dimensionless velocity between individual 1 and MEA;(b) Comparison of the dimensionless acceleration between individual 1 and MEA.

$$\frac{\partial r}{\partial u_1} \times \frac{\partial r}{\partial u_2} \cdot \frac{\partial r}{\partial \varsigma} = 0 \tag{15}$$

By combining Equations (14) and (15), we can solve for any one of the three parameters and substitute it into (14) to obtain the equation of the envelope surface in parameterized form. It is important to check for singularities, as the surface equation obtained through the above method may not always represent the envelope surface if singularities exist.

$$\frac{\partial r}{\partial u_1} \times \frac{\partial r}{\partial u_2} = 0 \tag{16}$$

If there are no singular points on the curve, then the curve must lie on the envelope surface, and along the curve, the surface is tangent to the envelope surface. Several such curves are referred to as characteristic curves of the surface family $\{S_\xi\}$. By utilizing these characteristic curves, it is possible to quickly establish the contact line equation between spatial cam surfaces and conical rolling elements.

By leveraging these characteristic curves, it becomes feasible to efficiently establish the contact line equation between spatial cam surfaces and conical rolling elements.

B. EQUATION OF SPATIAL CAMS

Based on (14) and the structural characteristics of the spatial cam mechanism, the angular displacement φ of the plunger shaft is chosen as the parameter ξ for the surface family. The distance δ from the conical rolling element's longitudinal section to the base plane and the angle θ of the rolling element are used as surface parameters u_1 and u_2, respectively, to describe the outer surface of the rolling element. (14) can be rewritten as:

$$r = r(\delta, \theta, \phi) \tag{17}$$

The mathematical model of the two-dimensional plunger-type electromechanical pump's spatial cam mechanism is illustrated in FIG 7.

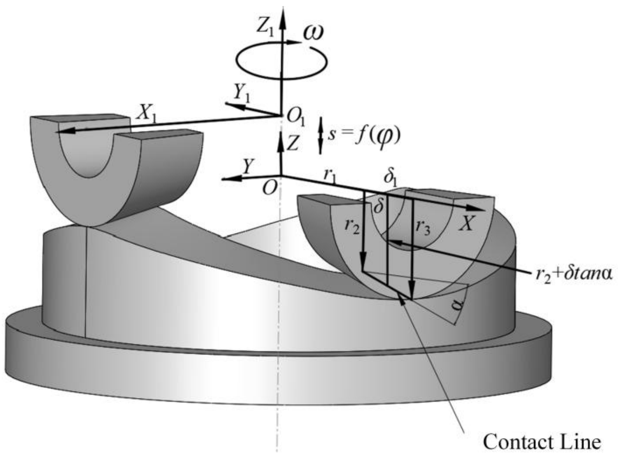

FIGURE 7. **Mathematical model of spatial CAM.**

In the mathematical model of the spatial cam mechanism of a two-dimensional plunger-type electromechanical pump, r_1 represents the distance from the base surface of the conical rolling element to the Z-axis of the fixed coordinate system. R_2 and r_3 are the radii of the upper and lower base surfaces of the conical rolling element, respectively, and δ_1 is the height of the conical rolling element. A denotes the apex angle of the conical rolling element. The radius of the circular cross-section located at a distance δ from the upper base surface of the conical rolling element is given by $r_2 + \delta\tan\alpha$. Φ represents the angular displacement of the plunger shaft, while the axial motion of the plunger shaft follows the law of $s = f(\varphi)$, where s is a function of the angular displacement.

By applying the principle of envelope in a single-parameter surface family and making coordinate transformations based on the aforementioned parameter settings, the equation of the surface family representing the outer surface of the conical rolling element in the fixed coordinate system can be obtained.

$$r = r(\delta, \theta, \phi) = \begin{bmatrix} \delta + r_1 \\ (r_2 + \delta \tan\alpha)\cos\theta \\ (r_2 + \delta\tan\alpha)\sin\theta + s \end{bmatrix}^T \times \begin{bmatrix} \cos\phi & -\sin\phi & 0 \\ \sin\phi & \cos\phi & 0 \\ 0 & 0 & 1 \end{bmatrix} \tag{18}$$

After simplification, we obtain:

$$\begin{bmatrix} x \\ y \\ z \end{bmatrix} = \begin{bmatrix} (\delta + r_1)\cos\phi + (r_2 + \delta\tan\alpha)\cos\theta\sin\phi \\ -(\delta + r_1)\sin\phi + (r_2 + \delta\tan\alpha)\cos\theta\cos\phi \\ (r_2 + \delta\tan\alpha)\sin\theta + s \end{bmatrix} \tag{19}$$

According to the principle of envelope for a single-parameter surface family, it is necessary to verify the existence of singular points in this parametric method. By substituting this parametric method into (16) and rearranging, we obtain:

$$\frac{\partial r}{\partial \delta} \times \frac{\partial r}{\partial \theta} = \begin{bmatrix} (r_2 + \delta\tan\alpha)(-\cos\theta\sin\phi + \tan\alpha\cos\phi) \\ -(r_2 + \delta\tan\alpha)(\cos\theta\cos\phi + \tan\alpha\sin\phi) \\ -(r_2 + \delta\tan\alpha)\sin\theta \end{bmatrix} \tag{20}$$

In (20), each term contains the coefficient $r_2 + \delta\tan\alpha$, which represents the radius of the longitudinal cross-section at a distance δ from the upper base of the rolling element. This value is always greater than zero, indicating that there are no singular points in the surface family. Therefore, this parametric method is valid.

By substituting the surface family represented by this parametric method into (15) and rearranging, we obtain:

$$\frac{\partial r}{\partial \delta} \times \frac{\partial r}{\partial \theta} \cdot \frac{\partial r}{\partial \phi} = -s'\sin\theta + (r_2 + \delta\tan\alpha)\tan\alpha\cos\theta + (\delta + r_1)\cos\theta = 0 \tag{21}$$

In this equation, θ is given by:

$$\theta = 2\arctan\left(\frac{-s' \pm \sqrt{s'^2 + (A\tan\alpha + B)^2}}{A\tan\alpha + B}\right) \tag{22}$$

In this equation, $A = r_2 + \delta\tan\alpha$, and $B = r_1 + \delta$.

By solving (21), we can obtain θ_1 and θ_2, which correspond to the surface parameters of the left and right spatial cam surfaces, respectively. These values can then be substituted into (19) to solve the mathematical model of the spatial cam mechanism and obtain the data points for the cam surface.

C. EQUATION OF SPATIAL CAMS

The shape of the cam surface in a spatial cam mechanism is complex. When constructing a three-dimensional model of the cam surface using discrete data points, it is necessary to first construct a spatial curve based on the point cloud and then establish the three-dimensional model. This process involves a large number of repetitive operations, and when the parameters are changed, the entire series of operations needs to be repeated. To facilitate obtaining the three-dimensional model of the spatial cam, a double cubic B-spline surface is used to interpolate the cam surface, and the interpolation results are used to generate a cam surface model file based on the data structure of the IGES file.

1) DOUBLE CUBIC B-SPLINE CAM SURFACE INTERPOLATION ALGORITHM

The B-spline surface is composed of multiple B-spline curves in the u and v directions and is determined by a control grid consisting of $(m+1)\times(n+1)$ control points. The equation of a $k\times l$ degree B-spline surface is:

$$p(u, v) = \sum_{i=0}^{m}\sum_{j=0}^{n} d_{i,j}N_{i,k}(u)N_{j,l}(v),\ u_k \leq u \leq u_{m+1},\ v_k \leq v \leq u_{n+1} \tag{23}$$

In (23), $d_{i,j}$ $(i = 0,1,\ldots, m;\ j = 0,1,\ldots, n)$ represents a set of control points. $N_{i,k}(u)$ $(i = 0,1,\ldots, m)$ and $N_{j,l}(v)$ are the normalized B-spline basis functions of degrees k and l, respectively, obtained from the knot vectors $U = (u_0, u_1,\ldots, u_{m+k+1})$ and $V = (v_0, v_1,\ldots, v_{n+l+1})$ using the de Boor-Cox recursion formula. Here, i and j are indices, and k and l represent the order of the B-spline curves in the u and v directions, respectively.

According to FIG 8, the reverse calculation of the control points for a double cubic B-spline surface can be divided into two stages.

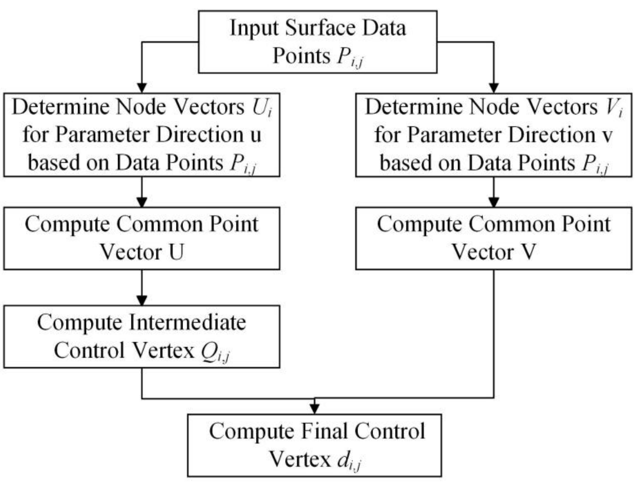

FIGURE 8. Reverse calculation process of the Bicubic B-Spline surface.

In the first stage, the data points in n-1 columns are interpolated separately on the knot vector U. Boundary conditions in the u-direction are applied to these columns of data points. By using the cubic B-spline interpolation algorithm, the intermediate control points $Q_{i,j}$ $(i = 0,1,\ldots, m,$ $j= 0,1,\ldots, n\text{-}2)$ are calculated. Each column of intermediate control points $Q_{i,j}$ contains 2 more points than the data point array $P_{i,j}$ in each column.

In the second stage, the m+1 rows of the intermediate control points $Q_{i,j}$ are treated as data points. Boundary conditions in the v-direction are applied to each row. By using the cubic B-spline interpolation algorithm again, the m+1 rows of data points are calculated on the knot vector V. This process yields the final set of control points $d_{i,j}(i = 0,1,\ldots, m; j = 0,1,\ldots, n)$ for the double cubic B-spline surface.

The specific steps for solving can be summarized as follows:

a: DETERMINATION OF THE PARAMETER DIRECTION

When solving for the data points on the cam surface using the principle of a single-parameter surface envelope, it is usually chosen to obtain the data points with equal angular spacing and equal axial spacing. The schematic diagram of the cam surface data point array, denoted as $P_{i,j}$, is shown in FIG 9.

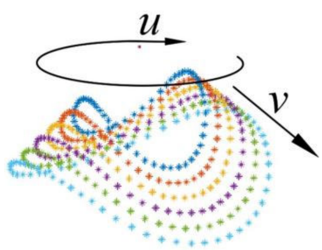

FIGURE 9. Data points of the cam surface.

According to the spatial distribution of data points, the circumferential direction is chosen as the u-parameter direction, and the axial direction is chosen as the v-parameter direction.

b: DETERMINATION OF SURFACE KNOT VECTORS

The knot vectors $U = (u_0, u_1,\ldots, u_{m+k+1})$ and $V = (v_0, v_1,\ldots, v_{n+l+1})$ for the B-spline interpolation surface are determined based on the parameterization of data points in the u and v directions.

First, for each of the ith B-spline interpolation curves in the u direction, the data points are parameterized using the accumulated chord length method and then normalized to obtain the knot vector $U_i = [u_{i,0}, u_{i,1},\ldots, u_{i,m+6}]$ $(i = 0,1,\ldots, n)$. The average value of the nodes with the same index from the obtained knot vectors is calculated as the node value for the corresponding index in the common knot vector U. The common knot vector U can be represented as:

$$U = \frac{1}{n+1}[\sum_{i=0}^{n} u_{i,0}, \sum_{i=0}^{n} u_{i,0}, \cdots, \sum_{i=0}^{n} u_{i,m+6}] \tag{24}$$

Similarly, the knot vectors V_i and the common knot vector V for the curves in the v direction can be obtained.

$$V_i = [v_{i,0}, v_{i,1}, \cdots, v_{i,n+6}](i = 0, 1, \cdots, m) \tag{25}$$

$$U = \frac{1}{m+1}[\sum_{i=0}^{m} u_{i,0}, \sum_{i=0}^{m} u_{i,0}, \cdots, \sum_{i=0}^{m} u_{i,m+6}] \tag{26}$$

c: CALCULATION OF THE INTERMEDIATE CONTROL POINTS $Q_{i,j}$

Interpolation is performed on the data points in n-1 columns using the knot vector U. Boundary conditions in the u direction are applied to each column of data points. The intermediate control points are obtained by using the reverse calculation algorithm for the cubic B-spline interpolation curve.

As shown in FIG 9, the curves formed by connecting the data points in each column in the u direction are closed curves. Based on the knowledge of B-spline interpolation curves, a cubic B-spline interpolation curve has n-1 equations and n+1 unknown control points. For a C^2 continuous cubic B-spline closed curve, the number of equations is reduced to n-2 because the initial and final data points p_0 and p_{n-2} are the same. Among the n+1 unknown points, the first and last three points are sequentially the same, i.e., $d_n = d_0, d_{n+1} = d_1, d_{n+2} = d_2$. This reduces the number of unknown points by three, leaving n-2 points. At this point, the number of unknown control points is equal to the number of equations, resulting in a unique solution. Therefore, for a cubic B-spline closed curve, there is no need to add additional constraint equations to solve for the control points. The linear system for reverse calculating the control points of the cubic B-spline curve based on the data points can be expressed in matrix form as follows.

$$\begin{bmatrix} b_0 & c_0 & & & a_0 \\ a_1 & b_1 & c_1 & & \\ & \ddots & \ddots & \ddots & \\ & & a_{n-2} & b_{n-2} & c_{n-2} \\ c_{n-1} & & & a_{n-1} & b_{n-1} \end{bmatrix} \begin{bmatrix} d_0 \\ d_1 \\ \vdots \\ d_{n-2} \\ d_{n-1} \end{bmatrix} = \begin{bmatrix} e_0 \\ e_1 \\ \vdots \\ e_{n-2} \\ e_{n-1} \end{bmatrix} \tag{27}$$

In this equation, the following can be obtained:

$$\begin{aligned} a_i &= \frac{(\Delta_{i+2})^2}{\Delta_i + \Delta_{i+1} + \Delta_{i+2}} \\ b_i &= \frac{\Delta_{i+2}(\Delta_i + \Delta_{i+1})}{\Delta_i + \Delta_{i+1} + \Delta_{i+2}} + \frac{\Delta_{i+1}(\Delta_{i+1} + \Delta_{i+3})}{\Delta_{i+1} + \Delta_{i+2} + \Delta_{i+3}} \\ c_i &= \frac{(\Delta_{i+1})^2}{\Delta_{i+1} + \Delta_{i+2} + \Delta_{i+3}} \\ e_i &= (\Delta_{i+1} + \Delta_{i+1})p_{i-1} \\ \Delta_i &= u_{i+1} - u_i, (0, 1, \cdots, n-3) \end{aligned}$$

d: CALCULATION OF THE FINAL CONTROL POINTS $d_{i,j}$

The intermediate control points $Q_{\mathrm{i,j}}$, with m+1 rows, are considered data points. Boundary conditions in the v direction are applied to each row, and the reverse calculation algorithm for cubic B-spline interpolation curves is used to interpolate these m+1 rows on the common knot vector V, resulting in the control points $d_{i,j}$.

As shown in FIG 9, the curves formed by connecting the data points in each row in the v direction are open curves. For a cubic B-spline open curve with a repetition degree of 4 at both ends, the initial and final control points are equal to the initial and final data points, i.e., $p_0 = d_0$ and $p_{n-2} = d_n$. This reduces the number of unknown points by 2, resulting in n-1 control points. With only n-3 equations, it is not possible to solve for n-1 unknown control points. Therefore, two additional boundary conditions need to be added to make the equation system have a unique solution. The linear equation system can be expressed in matrix form as follows:

$$\begin{bmatrix} b_1 & c_1 & a_1 & & \\ a_2 & b_2 & c_2 & & \\ & \ddots & \ddots & \ddots & \\ & & a_{n-2} & b_{n-2} & c_{n-2} \\ & & c_{n-1} & a_{n-1} & b_{n-1} \end{bmatrix} \begin{bmatrix} d_1 \\ d_2 \\ \vdots \\ d_{n-2} \\ d_{n-1} \end{bmatrix} = \begin{bmatrix} e_1 \\ e_2 \\ \vdots \\ e_{n-2} \\ e_{n-1} \end{bmatrix} \tag{28}$$

Common boundary conditions for open curves include tangent vector conditions, free endpoint conditions, phantom node conditions, parabolic conditions, and non-nodal conditions. In this study, the free endpoint condition is used as the boundary condition for the open curve in the v direction. Therefore, the coefficient calculation formulas in the first and last rows of the above equation can be expressed as follows:

$$\begin{cases} b_1 = \Delta_1 + 2\Delta_2 + 2\Delta_3 + \Delta_4 \\ c_1 = -(\Delta_1 + \Delta_2 + \Delta_3) \\ a_1 = 0 \\ e_1 = (\Delta_2 + \Delta_3 + \Delta_4)q_0 \end{cases} \tag{29}$$

$$\begin{cases} c_{n-1} = 0 \\ a_{n-1} = -(\Delta_n + \Delta_{n+1} + \Delta_{n+2}) \\ b_{n-1} = \Delta_{n-1} + 2\Delta_n + 2\Delta_{n+1} + \Delta_{n+2} \\ e_{n-1} = (\Delta_{n-1} + \Delta_n + \Delta_{n+1})q_{n-2} \end{cases} \tag{30}$$

By substituting the calculated common knot vectors U and V, as well as the control points $d_{i,j}$, into (23), the spatial cam surface can be obtained.

2) DATA STORAGE

The Initial Graphics Exchange Specification (IGES) is a universally defined information exchange standard by ANSI, which facilitates interchangeability between different CAD/CAM computer systems. Within this standard, various types of graphics are encoded, with type numbers 126 and 128 corresponding to rational B-spline curves and surfaces, respectively. As shown in FIG 10, the data of the spatial cam surface are stored in the directory entry section and parameter data section.

```
     128       1       0       0       0       0       0       0       0D      1
     128       0       0    2390       0                               0D      2
128,362,9,3,3,0,0,0,0,0,0.000000,0.000000,0.000000,0.000000,           1P      1
0.003814,0.007629,0.011444,0.015259,0.019076,0.022894,0.026713,        1P      2
0.030535,0.034358,0.038236,0.042053,0.045779,0.049393,0.052881,        1P      3
0.056240,0.059473,0.062591,0.065614,0.068562,0.071454,0.074304,        1P      4
0.077126,0.079932,0.082729,0.085524,0.088319,0.091116,0.093915,        1P      5
0.096716,0.099518,0.102321,0.105125,0.107929,0.110735,0.113540,        1P      6
0.116346,0.119151,0.121957,0.124762,0.127567,0.130372,0.133176,        1P      7
0.135980,0.138783,0.141585,0.144387,0.147188,0.149989,0.152789,        1P      8
```

FIGURE 10. Index section and parameter data section data.

Based on the relevant descriptions of the directory entry section and parameter data section format in "GB/T 14213-2008 Initial Graphics Exchange Specification," the following data, including the orders k and l in the u and v parameter directions, the number of control points (m+1 and n+1, respectively), the coordinates of each control point $d_{i,j}(i = 0,1,\ldots, m; j = 0,1,\ldots, n)$, the knot vectors U and V in the u and v directions, and the starting and ending parameter values u_k, u_{m+1}, v_l, and v_{n+1}, are sequentially written into an IGES format file. This file represents a cam surface model in IGES format.

V. CONSTRUCTION AND EXPERIMENT OF SPATIAL CAMS

A. TYPES OF GRAPHICS

The design process of a cam mechanism typically involves the following steps: 1. determining the motion law of the follower; 2. determining the type and structural dimensions of the cam mechanism; and 3. designing the CAM profile. The specific design process for a two-dimensional plunger-type hydraulic pump spatial cam mechanism is as follows:

1) DETERMINATION OF THE KEY PARAMETERS FOR THE CAM MECHANISM

The main parameters of the cam mechanism are shown in Table 2.

TABLE 2. Key parameters of the cam mechanism.

Parameters	Values(mm)	Parameters	Values(mm)
Inner Diameter of Tapered Roller	13	Tapered Roller Height	7
Outer Diameter of Tapered Roller	16	Inner Diameter of Cam	24
Plunger Shaft Stroke	5	Outer Diameter of Cam	38

2) DETERMINATION OF THE KINEMATIC LAWS FOR FOLLOWER MOTION

The B-spline optimized curve obtained in Section 2.4 is used to generate a cam model in Section III-C. This cam model is then incorporated into a spatial cam mechanism for kinematic simulation using Adams. The simulation results are compared in FIG 11 with the desired motion profiles of constant acceleration and deceleration, as well as the displacement, velocity, and acceleration profiles of the B-spline theory optimized curve, all within one cycle.

FIG 11 indicates that compared to the constant acceleration and deceleration transition modes, using the B-spline interpolation curve for the transition allows for seamless transition, avoiding rigid or flexible shocks at the transition points and ensuring the stability of the mechanism during high-speed operation. Due to its smooth and natural fitting characteristics, the B-spline curve reduces the losses and noise in bearings and transmission systems compared to the constant acceleration and deceleration motion profiles. Additionally, it effectively improves the transmission efficiency and service life of the mechanism.

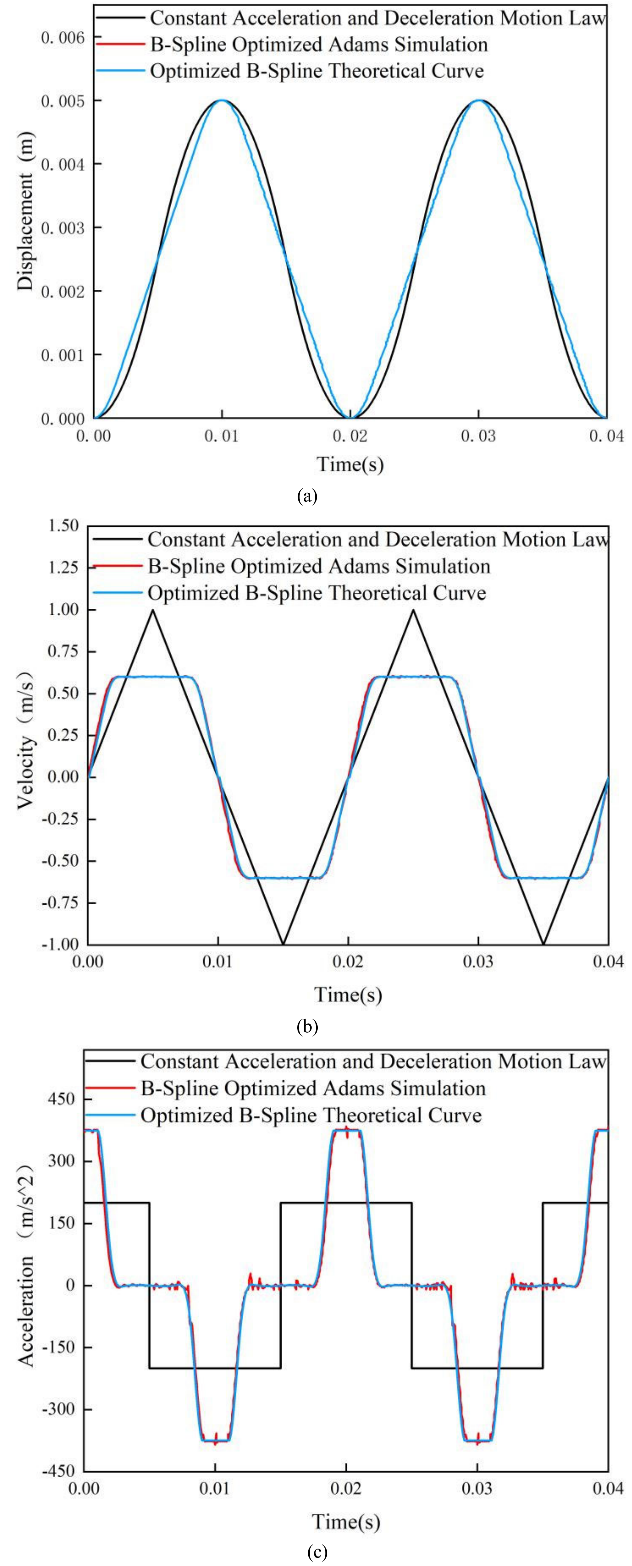

FIGURE 11. Comparison of the motion states(a) Displacement;(b) Velocity;(c) Acceleration.

FIG 11 shows the comparison between the B-spline theory optimized curve and the Adams simulation results based on B-spline optimization. The displacement, velocity, and acceleration curves of these three profiles are generally consistent. Although there is some fluctuation in the acceleration curve during abrupt changes, this fluctuation is reasonable and empirically validates the correctness of the cam curve design theory.

3) MATHEMATICAL MODELING

Using MATLAB tools, a mathematical model of the cam surface is established based on the motion law and key parameters of the cam mechanism. Relevant data, including point cloud data, cam surface data points, pressure angle, and curvature radius, are obtained. On the left side of FIG 12, the motion profile follows a constant acceleration and deceleration pattern, while on the right side, the motion profile follows the B-spline optimized curve.

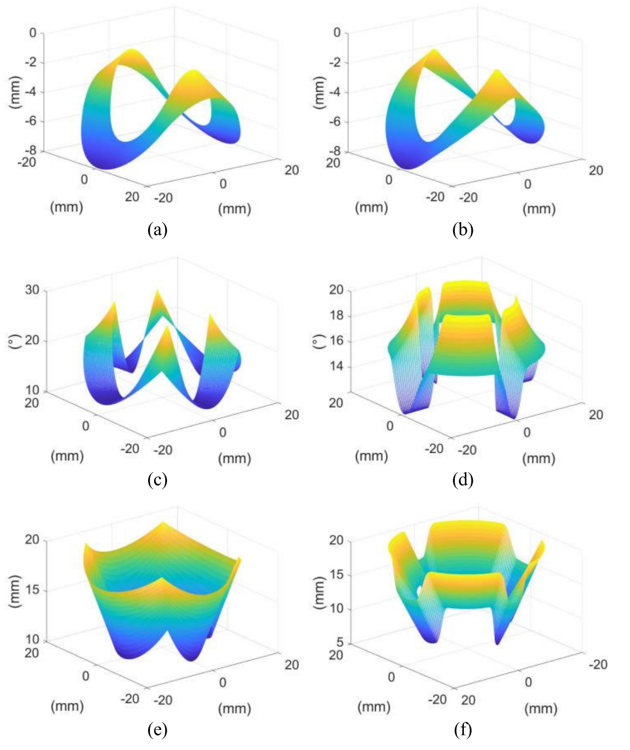

FIGURE 12. **Comparison of the cam parameters(a) Data points representing the cam surface based on the motion law of a constant acceleration and deceleration; (b) Data points representing the cam surface based on the motion law optimized with B-spline.; (c) Pressure angle of the cam based on the motion law of a constant acceleration and deceleration; (d) Pressure angle of the cam based on the motion law optimized with B-spline.; (e) Radius of curvature of the cam based on the motion law of a constant acceleration and deceleration.; (f) Radius of curvature of the cam based on the motion law optimized with B-spline.**

According to the displayed results in FIG 12 and Table 3, it can be observed that in the radial direction of the cam component, as the rotational radius increases, the pressure angle gradually decreases, while the curvature radius increases. The positions of the maximum pressure angle and minimum curvature radius are both located on the inner circle, corresponding to smaller rotational radii. The maximum pressure angle occurs at the midpoint of the forward or return motion. In the circumferential direction of the cam component, the minimum curvature radius is found at the extreme positions on the left and right sides, corresponding to larger rotational radii.

TABLE 3. **Key parameters of the cam mechanism.**

	Maximum Pressure Angle/°	Radius of Curvature
Constant Acceleration and Deceleration Motion Law	27.98	9.94
Optimized B-Spline Curve	19.92	7.44

4) GETTING A SURFACE MODEL

The point cloud data are processed using a bicubic B-spline interpolation algorithm, resulting in the surface control vertices $d_{i,j}$ and the knot vectors U and V.

The obtained surface information is written into an *IGES* format file to generate the cam surface model.

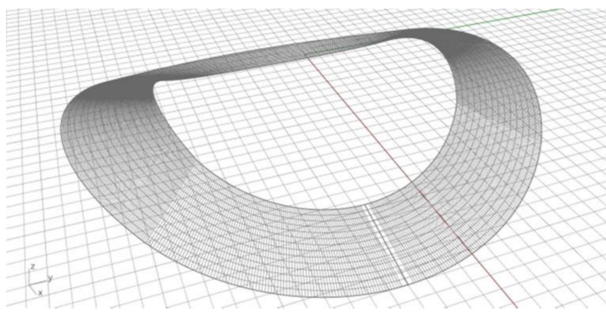

FIGURE 13. **Spatial cam surface model.**

The spatial cam surface model is then opened in Rhinoceros software, as shown in FIG 13.

In Rhinoceros software, the data point file generated by the program is imported as a point cloud into the spatial cam surface model. The point-deviation command is utilized to measure the distance between the point cloud and the surface model, generating corresponding error analysis and visualization results.

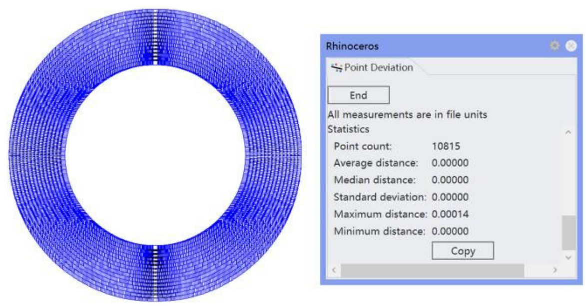

FIGURE 14. **Distance from the point cloud to the surface.**

As shown in FIG 14, the maximum distance between the point cloud and the surface is 0.00014 millimeters, while the minimum distance is 0 millimeters. In terms of mechanical machining, this difference can be considered negligible. The points with the largest deviations are located on the boundaries. This indicates that the bicubic B-spline cam surface interpolation algorithm can accurately calculate the B-spline representation of the cam surface based on the given surface data points. By storing the spline surface data in IGES format, we can obtain a feasible and accurate method for generating the spatial cam surface model.

5) COMPLETION OF MODELING

The cam surface model is imported into Rhinoceros software, and operations such as ''extrude surface'' are applied to obtain the solid cam model, as shown in FIG 15. This model can be exported in the desired format, such as SolidWorks or NX, which are commonly used mechanical 3D modeling software, for further design, analysis, and processing as needed.

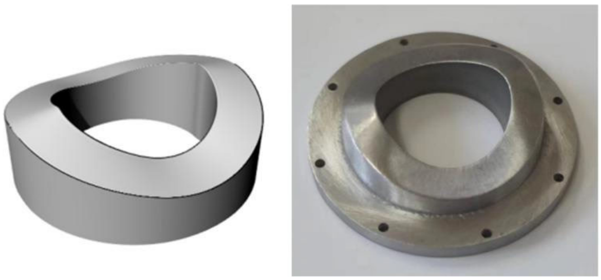

(a) (b)

FIGURE 15. Spatial cam model(a) 3D Model;(b) Machined prototype.

B. EXPERIMENTAL INVESTIGATION

The spatial cam mechanism is machined on a VMC850 three-axis vertical machining center. The components of this mechanism, including the spatial cam, cone roller shaft, and cone roller, are all made of 9Cr18Mo stainless steel. FIG 16 displays the physical prototype of the spatial cam mechanism.

FIGURE 16. Machined prototype.

Due to the two-dimensional motion of the plunger shaft, including the rotation and reciprocating motion, and its relatively small structural size, it is not feasible to directly

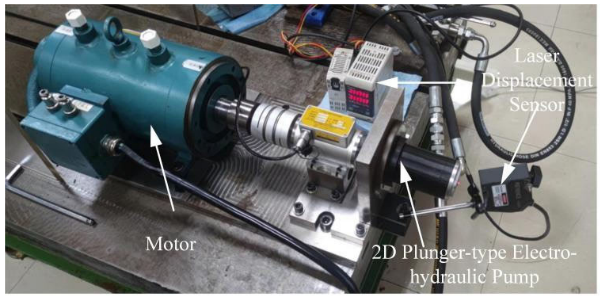

FIGURE 17. Displacement testing apparatus for the spatial cam mechanism.

install sensors on the plunger shaft to obtain velocity and acceleration information. To further validate the accuracy of the spatial cam surface, a laser displacement sensor can be employed to record the axial displacement curve of the plunger shaft, allowing for indirect verification. FIG 17 shows the corresponding testing setup.

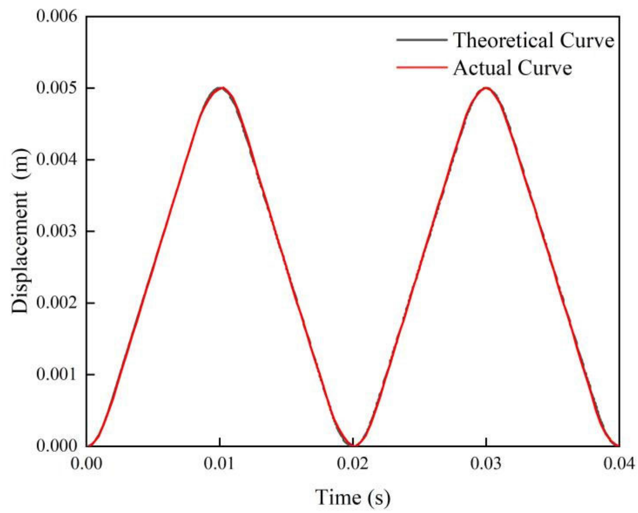

FIGURE 18. Comparison of the theoretical and actual displacement curves of plunger axis.

FIG 18 presents a comparison between the theoretical displacement curve and the actual displacement curve of the plunger shaft. The FIG indicates a generally good agreement between the theoretical and actual displacement curves of the plunger shaft. At the maximum deviation point, the difference is only approximately 0.161 millimeters near the two peaks, with an average deviation of approximately 0.095 millimeters. The manufactured spatial cam exhibits satisfactory machining accuracy, as evidenced by the displacement testing experiment of the spatial cam mechanism, demonstrating a good level of fit.

VI. CONCLUSION

In this paper, a design method for the cam motion curve in a two-dimensional plunger-type hydraulic pump cam mechanism is proposed. A fifth-order B-spline curve is used as a transition curve to achieve uninterrupted motion. The maximum dimensionless velocity and acceleration are considered optimization parameters. A multi-objective genetic algorithm is employed to optimize the motion curve, resulting in a Pareto solution set. The data points in the mathematical model are calculated using a bicubic B-spline cam surface interpolation algorithm, and the cam surface model file is generated in IGES file format. The cam mechanism is analyzed through simulations and experiments, leading to the following main conclusions:

(1)For the spatial cam mechanism of the two-dimensional plunger-type hydraulic pump, using a fifth-order B-spline curve as a transitional segment for uninterrupted motion can prevent the occurrence of continuous impacts during the transitional phase, thereby extending the lifespan of the mechanism.

(2)Compared to the MEA motion law, the B-spline composite motion law reduces the maximum velocity and acceleration characteristics by 1.39% and 0.86%, respectively, resulting in a motion law with good overall performance.

(3)A spatial cam design program is developed using the MATLAB GUI toolbox, enabling visualization of the cam mechanism design and reducing the difficulty and time required for design.

(4)The manufactured spatial cam exhibits satisfactory machining accuracy. The displacement testing experiment of the spatial cam mechanism shows a good level of fit, aligning closely with the theoretical design. The maximum deviation is only approximately 0.161 millimeters near the two peaks, with an average deviation of approximately 0.095 millimeters.

REFERENCES

[1] Y. Hu, S. Zhu, L. Xu, and B. Jiang, "Reduction of torque ripple and rotor eddy current losses by closed slots design in a high-speed PMSM for EHA applications," *IEEE Trans. Magn.*, vol. 58, no. 2, pp. 1–6, Feb. 2022, doi: 10.1109/TMAG.2021.3083664.

[2] F. Zhou, H. Liu, P. Zhang, X. Ouyang, L. Xu, Y. Ge, Y. Yao, and H. Yang, "High-precision control solution for asymmetrical electro-hydrostatic actuators based on the three-port pump and disturbance observers," *IEEE/ASME Trans. Mechatronics*, vol. 28, no. 1, pp. 396–406, Feb. 2023, doi: 10.1109/TMECH.2022.3200029.

[3] Z. Ma, H. Liao, J. Gao, S. Nie, and Y. Geng, "Physics-informed machine learning for degradation modeling of an electro-hydrostatic actuator system," *Rel. Eng. Syst. Saf.*, vol. 229, no. 3, pp. 42–43, Jan. 2023, doi: 10.1016/J.RESS.2022.108898.

[4] J. Fang, X. Wang, R. Li, S. Wang, and W. Wang, "Active ankle prosthesis powered by electrohydrostatic actuation technology: Design and implementation," in *Proc. CSAA/IET Int. Conf. Aircr. Utility Syst. (AUS)*, Guiyang, China, Jun. 2018, pp. 1170–1175, doi: 10.1049/cp.2018.0177.

[5] C. Ding, Y. Zhu, L. Liu, C. Tong, and J. Ruan, "Research on a novel flowmeter with parallel two-dimensional pistons as its metering units," *IEEE Access*, vol. 7, pp. 110912–110927, 2019, doi: 10.1109/ACCESS.2019.2933662.

[6] T. Xing, X. Yan, Y. Huang, C. Gao, and J. Ruan, "Outlet pressure and flow characteristics of a new two-dimensional piston pump with an overlapped distributor," *Energies*, vol. 16, no. 11, p. 4303, May 2023, doi: 10.3390/EN16114303.

[7] P. Tomov and D. Yanulov, "Dynamic model of electro-hydraulic pumping unit driven by an asynchronous motor," in *Proc. 21st Int. Symp. Electr. App. Technol. (SIELA)*, Bourgas, Bulgaria, Jun. 2020, pp. 1–4, doi: 10.1109/SIELA49118.2020.9167070.

[8] K.-M. Lee, L. Li, K. Bai, X. Ouyang, and H. Yang, "Harmonic model and remedy strategy of multiphase PM motor under open-circuit fault," *IEEE/ASME Trans. Mechatronics*, vol. 24, no. 3, pp. 1407–1419, Jun. 2019, doi: 10.1109/TMECH.2019.2906850.

[9] K. R. Khan and M. S. Miah, "Fault-tolerant BLDC motor-driven pump for fluids with unknown specific gravity: An experimental approach," *IEEE Access*, vol. 8, pp. 30160–30173, 2020, doi: 10.1109/ACCESS.2020.2972942.

[10] K. H. Dawoud and A. M. Abu-Hudrouss, "Off-grid solar photovoltaic BLDC motor pumping technology for irrigation in gaza strip," in *Proc. 8th Int. Eng. Conf. Renew. Energy Sustainability (ieCRES)*, Gaza, Palestine, May 2023, pp. 1–5, doi: 10.1109/ieCRES57315.2023.10209522.

[11] Y. Noh, W. Kim, and J. Lee, "Online short-circuit protection strategy of an electric powerpack for electric oil pump applications," *IEEE Access*, vol. 9, pp. 52292–52309, 2021, doi: 10.1109/ACCESS.2021.3069454.

[12] M. Kilani, H. Khasawneh, A. Badran, and A. Awidi, "Further development on a gentle electromagnetic pump for fluids with stress-sensitive microparticles," *Sens. Actuators A, Phys.*, vol. 247, pp. 440–447, Aug. 2016, doi: 10.1016/j.sna.2016.06.031.

[13] Y. Huang, L. Liu, W. Shao, W. Yu, and C. Ding, "Numerical and experimental study on flat roller/cam pair in a two-dimensional piston pump," *Tribol. Int.*, vol. 188, Oct. 2023, Art. no. 108823, doi: 10.1016/j.triboint.2023.108823.

[14] L. Lu, Y. Chen, C. Tong, J. Ruan, and S. Li, "Design strategy and performance evaluation of novel miniature two-dimensional (2D) piston pump with a dual stacking mechanism," *Alexandria Eng. J.*, vol. 62, pp. 541–554, Jan. 2023, doi: 10.1016/J.AEJ.2022.07.049.

[15] F. Y. Chen, *Mechanics and Design of Cam Mechanisms*. New York, NY, USA: Pergamon, 1982.

[16] J. Angeles, "Synthesis of plane curves with prescribed local geometric properties using periodic splines," *Comput.-Aided Des.*, vol. 15, no. 3, pp. 147–155, May 1983, doi: 10.1016/0010-4485(83)90081-7.

[17] D. M. Tsay and B. J. Lin, "Improving the geometry design of cylindrical cams using nonparametric rational B-splines," *Comput.-Aided Des.*, vol. 28, no. 1, pp. 5–15, Jan. 1996, doi: 10.1016/0010-4485(95)00020-8.

[18] H. Qiu, C.-J. Lin, Z.-Y. Li, H. Ozaki, J. Wang, and Y. Yue, "A universal optimal approach to cam curve design and its applications," *Mechanism Mach. Theory*, vol. 40, no. 6, pp. 669–692, Jun. 2005, doi: 10.1016/j.mechmachtheory.2004.12.005.

[19] D. M. Tsay and H. M. Wei, "A general approach to the determination of planar and spatial cam profiles," *J. Mech. Design*, vol. 118, no. 2, pp. 259–265, Jun. 1996, doi: 10.1115/1.2826878.

[20] D.-C. Jin, J. Ruan, S. Li, B. Meng, and L.-F. Wang, "Modelling and validation of a roller-cam rail mechanism used in a 2D piston pump," *J. Zhejiang Univ.-Sci. A*, vol. 20, no. 3, pp. 201–217, Mar. 2019, doi: 10.1631/jzus.A1800085.

[21] J. Huang, P. Hu, K. Wu, and M. Zeng, "Optimal time-jerk trajectory planning for industrial robots," *Mechanism Mach. Theory*, vol. 121, pp. 530–544, Mar. 2018. [Online]. Available: https://www.sciencedirect.com/science/article/pii/S0094114X17302914

[22] K. Deb, A. Pratap, S. Agarwal, and T. Meyarivan, "A fast and elitist multiobjective genetic algorithm: NSGA-II," *IEEE Trans. Evol. Comput.*, vol. 6, no. 2, pp. 182–197, Apr. 2002, doi: 10.1109/4235.996017.

[23] D. Martín, A. Rosete, J. Alcalá-Fdez, and F. Herrera, "QAR-CIP-NSGA-II: A new multi-objective evolutionary algorithm to mine quantitative association rules," *Inf. Sci.*, vol. 258, pp. 1–28, Feb. 2014, doi: 10.1016/j.ins.2013.09.009.

XINGUO QIU received the M.Sc. and Ph.D. degrees from the Zhejiang University of Technology, in 2005 and 2009, respectively.

He is currently a Senior Engineer and a Master Supervisor with the Zhejiang University of Technology. He has presided over more than 20 national key unit projects, the National Natural Science Foundation of China, the Research and Development Projects of Zhejiang Province, applied for more than 200 patents, and has been granted more than 100 national patents, with more than 40 patents granted to the first inventor, more than 20 papers with SCI/EI indexed papers, and EI included more than 20 papers. His research interests include fluid transmission and control, electromechanical servo control, and near field acoustic holography in sound and vibration. He serves as an Expert of the National Natural Science Foundation of China, a member of the Fluid Control Engineering Committee of the Chinese Society of Mechanics, and a Senior Member of the Chinese Society of Mechanical Engineering.

FUCHENG WANG is currently pursuing the master's degree in mechanical engineering with the Zhejiang University of Technology, Hangzhou, China. His research interests include motor servo control, fluid transmission and control, and visual fatigue detection.

CHANGLONG LI is currently pursuing the M.S. degree in mechanical engineering with the Zhejiang University of Technology, Hangzhou, China. His research interests include optimized design of pump, optimized design of integrated motor, and pump structure.

BIDA YI received the bachelor's degree in mechanical engineering from the Zhejiang University of Technology, in 2023. His research interests include motor servo control, fluid transmission and control, and visual fatigue detection.

JIAN RUAN received the B.S., M.S., and B.S. degrees in fluid power transmission and control from the Harbin Institute of Technology, Harbin, China, in 1983, 1986, and 1989, respectively, and the Postdoctoral degree in fluid power transmission and control from the Research Institute, Zhejiang University, Zhejiang, China, in 1992.

He is currently the Director of the 2D Hydraulic/Pneumatic Components and Systems Engineering Technology Research Center, Zhejiang University of Technology (ZJUT). He has presided over one project of the National Key Research and Development Program, six projects of National Natural Science Foundation of China, three projects of National Defense Science and Technology Innovation Special Zone of Science and Technology Commission of the Central Military Commission, and one major horizontal project of 10 million dollars.

Prof. Ruan is also an Executive Member of Fluid Transmission and Control Branch of Chinese Mechanical Engineering Society and a member of Fluid Transmission and Control Branch of Chinese Aeronautical Society.

WEI JIANG received the bachelor's and master's degrees in mechanical engineering from Zhejiang University, in 1983 and 1990, respectively, and the Ph.D. degree from the Zhejiang University of Technology.

He was the Director of the Mechanical Design Teaching and Research Department, the Director of the Institute of Measurement and Control Technology and Instrumentation, the Deputy Dean of the School of Mechanical Engineering, the Deputy Dean of the Institute of Science and Technology Research, and is currently a Professor with the School of Mechanical Engineering and a Doctoral Supervisor with the Zhejiang University of Technology (ZJUT). He has long been engaged in teaching and research work in the direction of fluid transmission and control, mechatronics equipment, and special equipment. As the project leader, he has been awarded eight national equipment pre-research projects, two national equipment development projects, two scientific research products into the model, and more than 20 horizontal scientific research projects. He has been awarded more than ten patents for invention and published dozens of academic papers of various types and has been awarded the first prize of the Science and Technology Prize of China Machinery Industry.